




## RESEARCH ARTICLE OPEN ACCESS

# Post-Transcriptional Regulation of Rab7a in Lysosomal Positioning and Drug Resistance in Nutrient-Limited Cancer Cells

Aliye Ezgi Güleç Taşkiran<sup>1,2</sup>  | Hepşen H. Hüsniğil<sup>1</sup> | Zahra E. Soltani<sup>3</sup> | Göksu Oral<sup>1</sup> | Nazlı S. Menemenli<sup>1</sup> | Chuanpit Hampel<sup>4</sup> | Kerstin Huebner<sup>4</sup> | Katharina Erlenbach-Wuensch<sup>4</sup> | Ilir Sheraj<sup>1</sup> | Regine Schneider-Stock<sup>4,5</sup> | Aytekin Akyol<sup>6</sup> | Nalan Liv<sup>3</sup>  | Sreeparna Banerjee<sup>1,7</sup> 

<sup>1</sup>Department of Biological Sciences, Orta Dogu Teknik Universitesi, Ankara, Turkiye | <sup>2</sup>Department of Molecular Biology and Genetics, Başkent University, Ankara, Turkiye | <sup>3</sup>Center for Molecular Medicine, University Medical Center Utrecht, Utrecht University, Utrecht, Netherlands | <sup>4</sup>Experimental Tumor Pathology, Institute of Pathology, University Hospital Erlangen, Friedrich Alexander University Erlangen-Nürnberg, Erlangen, Germany | <sup>5</sup>Comprehensive Cancer Center Erlangen-EMN (CCC ER-EMN), Bavarian Cancer Research Center (BZKF), Erlangen, Germany | <sup>6</sup>Department of Pathology, Hacettepe University Faculty of Medicine, Ankara, Turkey | <sup>7</sup>Cancer Systems Biology Laboratory (CanSyL), Orta Dogu Teknik Universitesi, Ankara, Turkiye

**Correspondence:** Sreeparna Banerjee ([banerjee@metu.edu.tr](mailto:banerjee@metu.edu.tr))

**Received:** 16 January 2024 | **Revised:** 17 July 2024 | **Accepted:** 3 September 2024

**Funding:** This work was supported by Orta Doğu Teknik Üniversitesi, Türkiye Bilimsel ve Teknolojik Araştırma Kurumu, European Molecular Biology Organization and TUBITAK BİDEB.

**Keywords:** chemoresistance | drug trapping | lysosome | nutrient limitation | Rab7a

## ABSTRACT

Limited nutrient availability in the tumor microenvironment can cause the rewiring of signaling and metabolic networks to confer cancer cells with survival advantages. We show here that the limitation of glucose, glutamine and serum from the culture medium resulted in the survival of a population of cancer cells with high viability and capacity to form tumors in vivo. These cells also displayed a remarkable increase in the abundance and size of lysosomes. Moreover, lysosomes were located mainly in the perinuclear region in nutrient-limited cells; this translocation was mediated by a rapid post-transcriptional increase in the key endolysosomal trafficking protein Rab7a. The acidic lysosomes in nutrient-limited cells could trap weakly basic drugs such as doxorubicin, mediating resistance of the cells to the drug, which could be partially reversed with the lysosomal inhibitor bafilomycin A1. An in vivo chorioallantoic membrane (CAM) assay indicated a remarkable decrease in microtumor volume when nutrient-limited cells were treated with 5-Fluorouracil (5-FU) and bafilomycin A1 compared to cells treated with either agent alone. Overall, our data indicate the activation of complementary pathways with nutrient limitation that can enable cancer cells to survive, proliferate and acquire drug resistance.

## 1 | Introduction

Cancer cells need to rewire their metabolism and activate both catabolic and anabolic pathways to cope with the energetic, nutritional and biosynthetic requirements of rapid proliferation [1]. Consequently, these cells take up large amounts of nutrients such as glucose and glutamine to support growth. Metabolic

intermediates generated during glycolysis and the tricarboxylic acid (TCA) cycle supply building blocks for the synthesis of nucleic acids, amino acids and fatty acids [2]. Glutamine catabolism maintains a steady supply of nutrients into the TCA cycle (anaplerosis), thus preserving its integrity despite a continual efflux of metabolites (cataplerosis) to support growth [3]. Although aberrant cellular metabolism was reported in cancer

This is an open access article under the terms of the [Creative Commons Attribution-NonCommercial](https://creativecommons.org/licenses/by-nc/4.0/) License, which permits use, distribution and reproduction in any medium, provided the original work is properly cited and is not used for commercial purposes.

© 2024 The Author(s). *Traffic* published by John Wiley & Sons Ltd.

cells nearly a century ago, rewiring of metabolic pathways has only recently been recognized as an emerging hallmark of cancer [4].

The tumor environment can be limiting in both nutrients and oxygen, especially when the vasculature is poorly developed [5]. In such situations, cells induce autophagy to recycle macromolecules through the elimination of long-lived, aggregated and misfolded proteins or damaged organelles [6]. Lysosomes, which are highly acidic organelles containing more than 60 different hydrolases, play a major role in the degradation of autophagic vesicles [7]. Since cancer cells proliferate rapidly, their demand for nutrients is high, and their uncontrolled growth leads to the accumulation of aggregated proteins, damaged organelles etc., which are recycled by the lysosomes [8]. At the same time, the macromolecules released from lysosomes can serve as building blocks to promote biomass production [9].

Lysosomes can also regulate cellular response to chemotherapy. Lysosomal trapping is defined as the sequestration of lipophilic, or weakly basic drugs in lysosomes via nontransporter-mediated mechanisms, where the drugs can get inactivated [10, 11]. Previous studies suggest that anticancer agents can accumulate in perinuclear lysosomes [12, 13]. Moreover, lysosomal inhibitors such as the v-ATPase inhibitor bafilomycin A1 [7] can interfere with lysosomal acidity and/or the activity of lysosomal enzymes and enhance the effects of chemotherapy agents. In gastric cancer, the combination of bafilomycin A1 with 5-fluorouracil (5-FU) was shown to enhance the effect of 5-FU [14], while in multiple myeloma, it was shown to enhance the activity of bortezomib [14, 15]. Chloroquine, a lysosomotropic agent, was shown to sensitize mouse breast cancer cells to cisplatin [16] and human glioblastoma cells to temozolomide [17].

Standard cell culture media do not reflect nutrient availability in the tumor microenvironment; rather, they reflect the most appropriate medium required for cells to grow. To better reflect the physiological limitation of major nutrient sources in the tumor microenvironment, we used a cell culture medium containing 10% of the nutrients found in the complete culture medium. We have previously shown that the limitation of major nutrient sources such as glucose, glutamine and serum resulted in a population of cells that were highly viable, motile and tumorigenic in vivo and showed the activation of a partial EMT program [18, 19]. Additionally, nutrient-limited colon cancer cells expressed a three-gene signature (*EGFR*, *SOX10*, *SERPINE A1*) that could predict poor prognosis across multiple patient cohorts [19]. In the current study, we show that nutrient-limited cells could activate signaling pathways that enhanced lysosomal numbers, acidity and activity. Additionally, a rapid miRNA-mediated post-transcriptional upregulation of the late endosomal marker Rab7a orchestrated the perinuclear localization of the lysosomes. We show that these perinuclear lysosomes could trap drugs, causing the cells to acquire resistance to chemotherapy agents providing a novel mechanism for drug resistance induced by nutrient limitation. Resistance to drugs such as 5-FU and doxorubicin could be partially reversed with the use of lysosomal inhibitors, such as bafilomycin A1, highlighting the clinical relevance of our observations.

## 2 | Results

### 2.1 | Nutrient Limitation Selects for Cells With High Viability Under Nutrient Scarcity

The primary response of cells to nutrient limitation is the activation of energy-sensing pathways and induction of autophagy to accommodate the changes in nutrient availability [20]. We evaluated whether the incubation of a panel of CRC cell lines in a nutrient-limited medium containing 10% of the nutrients found in the complete medium led to the activation of nutrient-sensing pathways and autophagy. AMPK was phosphorylated at T172, whereas the mTOR pathway was inhibited in all cell lines as evidenced by decreased phosphorylation of p70S6 Kinase at Thr389 and/or 4EBP1 at Ser65 in response to nutrient limitation (Figure 1A). The induction of autophagy was also observed in all cell lines as shown by the increased level of LC3-II, although we observed an increase in the overall levels of the cargo protein p62 (Figure 1B). To evaluate whether flux was inhibited in these cells, we treated Caco-2, LoVo and T84 cells with bafilomycin A1, which decreases the acidity of lysosomes and therefore interferes with lysosomal degradation [21]. We observed that Caco-2 and LoVo cells treated with bafilomycin A1 led to the robust accumulation of p62 and LC3-II in both nutrient-rich and nutrient-limited cells, indicating the presence of autophagic flux in these cell lines (Figure S1A). T84 cells showed a modest accumulation of p62 with bafilomycin A1, especially in the nutrient-rich cells, suggesting that flux was slower in these cells, although the accumulation of LC3-II was comparable across all cell lines (Figure S1A). All cell lines after 48 h of nutrient limitation showed high viability (Figure S1B). T84 cells showed the ability to form microtumors of comparable volume with nutrient-rich and limited medium in vivo (Figure 1C). We have previously reported comparable microtumor volumes with LoVo and Caco-2 cells grown in nutrient-rich and -limited medium [18]. Staining for Ki67 (a human tumor cell cycle-related marker) of the microtumors generated from nutrient-rich and -limited cells was also comparable, indicating the high viability of the cells in vivo (Figure 1D).

### 2.2 | Lysosomal Activity in Nutrient-Limited Cells

The induction of autophagy is associated with the activation of lysosomal degradation of autophagic cargo [22]. To determine whether incubation of the three cell lines in the nutrient-limited medium affected the acidification and activation of lysosomes we used siRLysosome, a cell-permeable fluorescent reporter-conjugated peptide that is known to bind specifically to active cathepsin D in the lysosome. We observed a significant increase in the siRLysosome signal in nutrient-limited T84 cells, while the same was not observed with Caco-2 and LoVo cells (Figure 2A,B). Incubation of the cells with bafilomycin A1 led to a robust decrease in the siRLysosome signal in all cell lines, as expected. Supporting the siRLysosome data, T84 (but not Caco-2) cells, showed significantly higher LysoTracker signal in response to nutrient limitation (Figure S1C,D) suggesting either the presence of more acidic or a greater number of lysosomes in T84 cells. Caco-2 cells did not show a significant change in the LysoTracker signal in response to nutrient limitation most likely due to unchanged acidity of lysosomes; we have previously shown no change in lysosome numbers with nutrient limitation in Caco-2 cells [18]. The LysoTracker signal

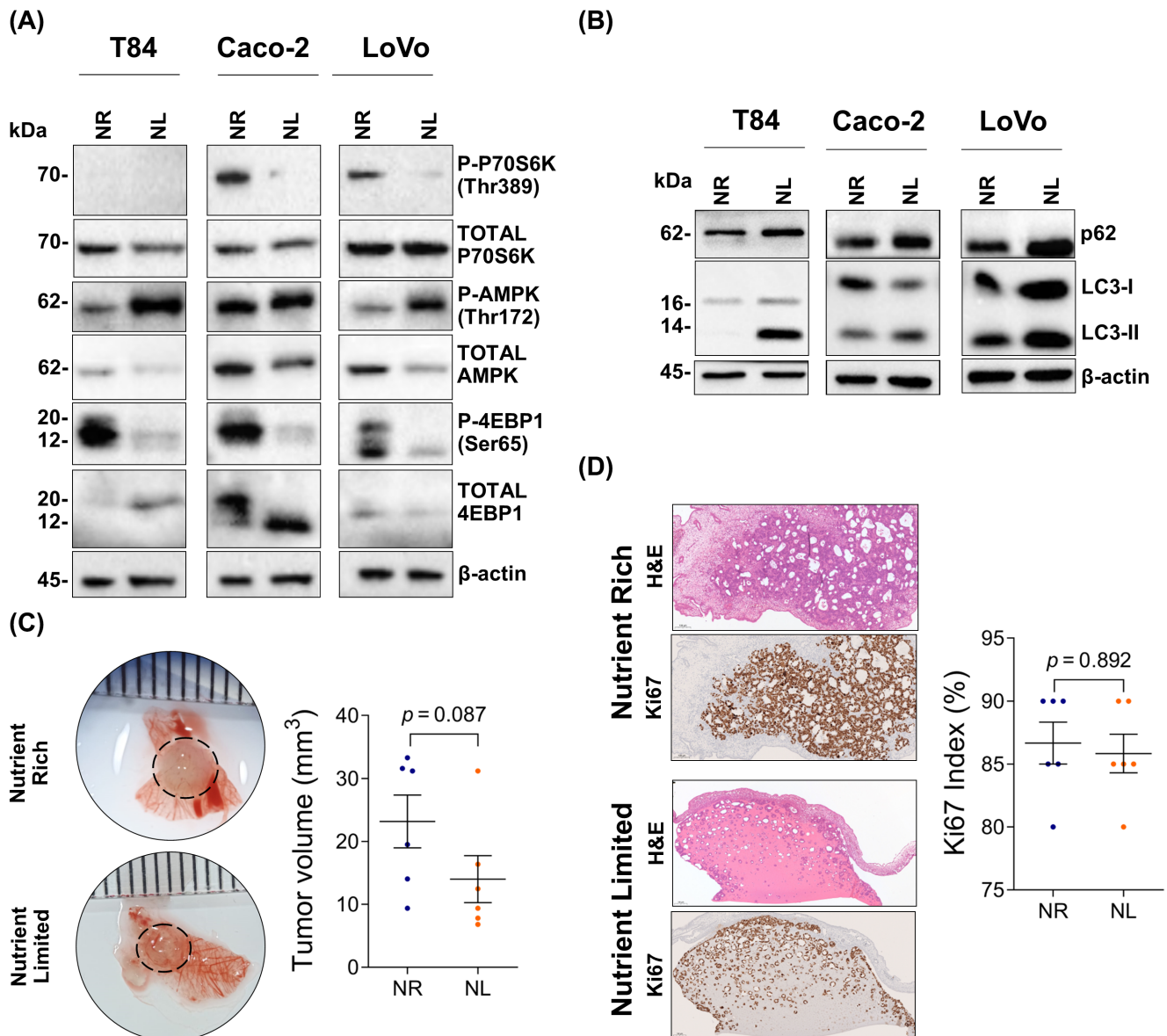


**FIGURE 1** | Effect of nutrient limitation on the activation of nutrient-sensing pathways, autophagy and tumor-forming ability of colorectal cancer cells. (A, B) T84, Caco-2 and LoVo cells were incubated in a nutrient-limited medium containing 10% of the nutrients found in a complete medium for 48 h and processed for western blot. Images are representative of three independent biological replicates.  $\beta$ -Actin was used as an internal control for equal protein loading, bands generated with antibodies against the total antigen were used for normalization if applicable, and fold changes were determined based on this normalization. Densitometry analyses are shown in Figure S4. (C) Representative microtumor images from nutrient-rich and -limited cells are shown in the left panel. Volume data from six microtumors from both nutrient-rich and -limited T84 cells are shown in the right panel. (D) Representative images of hematoxylin and eosin (H&E) and Ki-67 staining of T84 cell microtumors are given in the left panel. The scanned images of CAM sections were taken at 20 $\times$  magnification, scale bar: 50 $\mu$ m. Images are representative of six different microtumor samples per group. The Ki67 Index (%) of six microtumors is given in the right panel. The tumors were excised and embedded in paraffin followed by sectioning, deparaffinization and staining. Statistical analysis was carried out using Mann–Whitney  $U$  test. NL, nutrient-limited; NR, nutrient-rich.

was remarkably low in LoVo cells in both nutrient-rich and limited cells, therefore we were unable to assess lysosomal acidity (data not shown). To further substantiate our findings of increased lysosomal activity in T84 cells, we have carried out a western blot for mature (cleaved) and pro-cathepsin B (Figure 2C). We observed an increase in mature cathepsin B in T84 cells with nutrient limitation, but not in Caco-2 cells. LoVo cells had a remarkably low expression of cathepsin B. Treatment with bafilomycin A1 led to a decrease in the levels of mature and pro-cathepsin B in both nutrient-rich and -limited media in all cell lines (Figure 2C). p62 is a cargo

protein that is degraded in the lysosome during autophagy and its degradation is indicative of functional lysosomes. We treated T84 cells with bafilomycin A1 for 48 h. Following this, the cells were either collected directly, or the bafilomycin A1-containing medium was removed, and the cells were washed and allowed to recover in the nutrient-rich medium for 24 h (labeled as bafilomycin A1 recovery). T84 cells showed accumulation of the p62 cargo protein upon nutrient limitation, which was further enhanced upon treatment of the cells with bafilomycin A1 (Figure S1E), followed by a decrease when the bafilomycin A1 treatment was withdrawn. This suggests that

T84 cells have functional lysosomes that are capable of degrading their cargo. Next, we carried out an immunofluorescence (IF) assay to determine the localization of the lysosomal enzyme

cathepsin D and the lysosomal membrane marker LAMP1 in T84 cells. We observed that both nutrient-rich and limited T84 cells displayed moderate (Pearson's coefficient > 0.71)

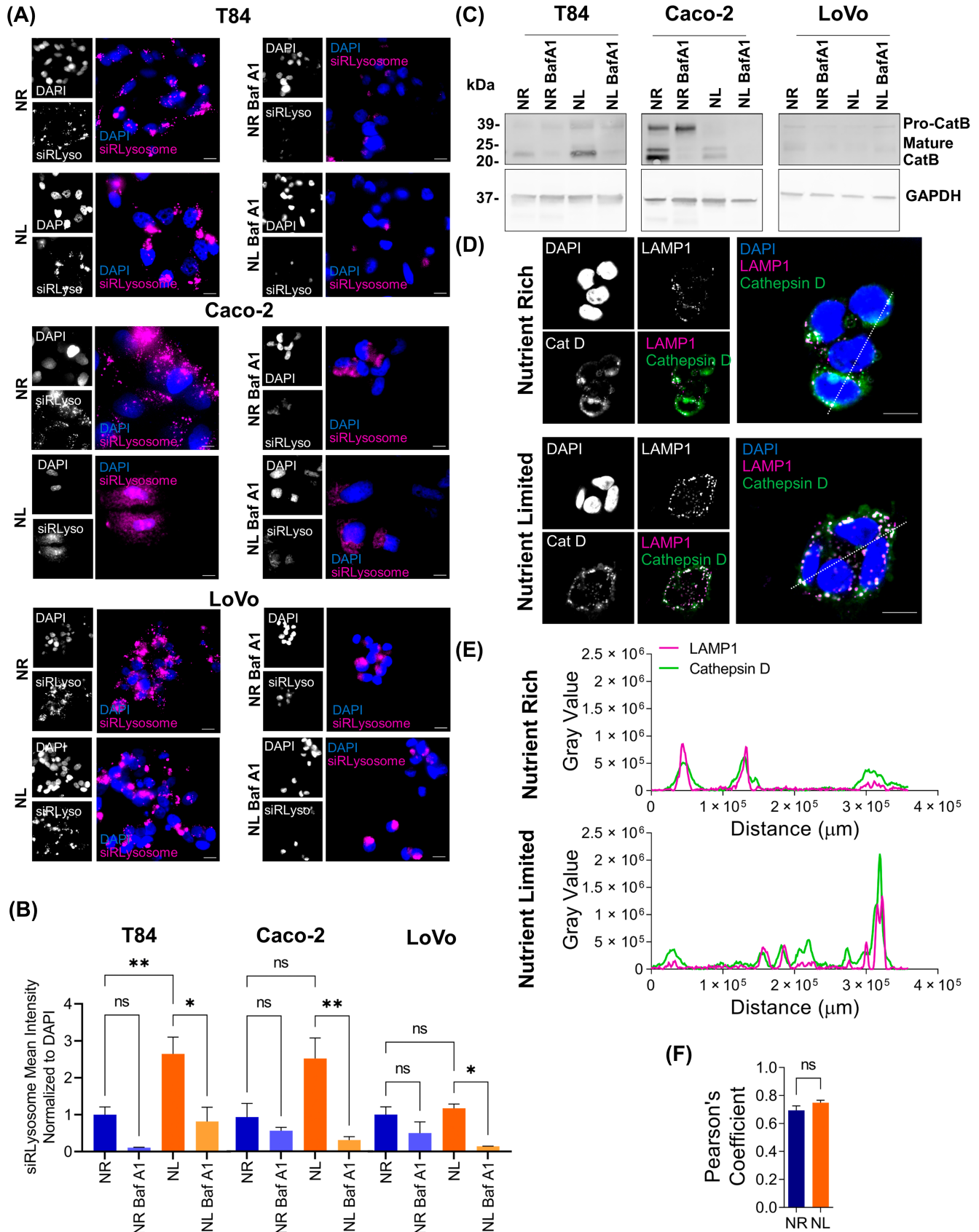


**FIGURE 2** | Figure legend on next page.



colocalization of cathepsin D and LAMP1, indicating that cathepsin D was localized at its site of activity in nutrient-limited T84 cells (Figure 2D) [23]. Additionally, intensity profiles along a line traced over the image for both nutrient-rich

and -limited cells showed that the peaks of both LAMP1 and cathepsin D were closely aligned, suggesting the presence of active degradative lysosomes (Figure 2E). The colocalization of LAMP1 and cathepsin D did not show any significant

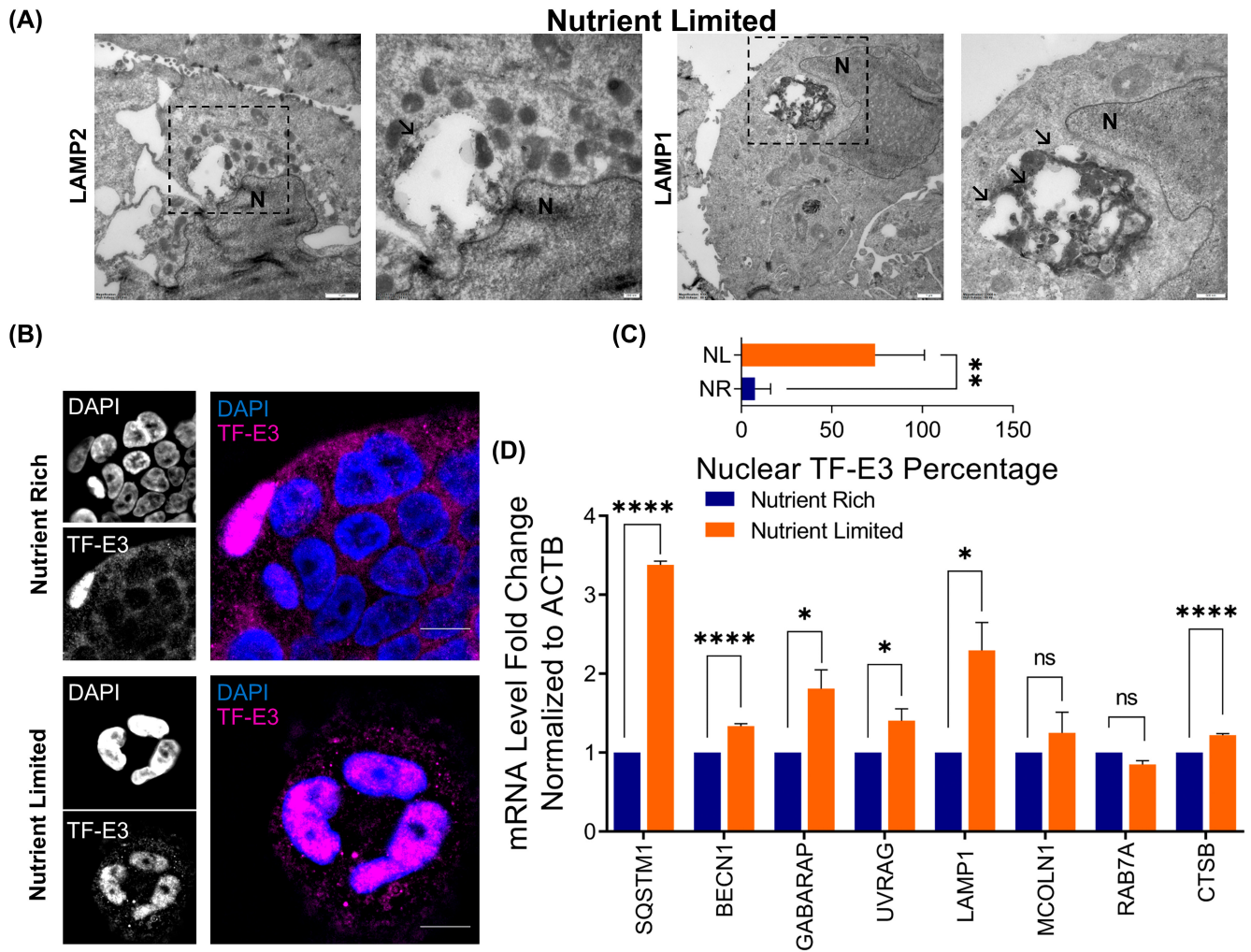


**FIGURE 3** | Evaluation of the effects of nutrient limitation on lysosome abundance and/or biogenesis in T84 cells. (A) T84 cells were treated for 24h in a nutrient-limited medium and processed for immuno-EM as described in materials and methods. Lysosomes were labeled with antibodies against the lysosomal membrane markers LAMP1 and LAMP2. Scale bars correspond to 1  $\mu$ m for images in the left panel and 500 nm (for LAMP1) and 250 nm (for LAMP2) for the images in the right panel. The regions highlighted with rectangles in the left panel images are shown in higher magnification in the right panel. The arrows indicate the lysosomes, and N refers to the nucleus. (B) T84 cells were incubated in a nutrient-rich or -limited medium for 24h and processed for immunofluorescence staining for TF-E3. The scale bars correspond to 10  $\mu$ m. (C) The nuclear percentage was determined using the ratio of cells with nuclear TF-E3 to whole cell number. A total of 5 images and 50 cells from each group were used for the analysis. (D) The mRNA-level expression of a selected group of CLEAR genes was determined by qRT-PCR. *ACTB* was used as an internal control, and fold changes were determined by normalization to nutrient-rich cells. Statistical analysis was carried out using an unpaired student *t*-test. \* $p < 0.05$ , \*\* $p < 0.01$ , \*\*\*\* $p < 0.0001$ ; NL, nutrient-limited; NR, nutrient-rich; ns, nonsignificant.

**FIGURE 2** | Evaluation of the effects of nutrient limitation on lysosomal acidity and degradative activity. (A, B) Nutrient-rich or 48h nutrient-limited cells were stained with siRLysosome for 3h at 37°C. Nutrient-rich or 48h nutrient-limited cells were also treated for 48h with 50nM bafilomycin A1. The cell numbers were normalized to DAPI staining. Fold changes of two biological replicates with respect to nutrient-rich cells are given as mean  $\pm$  SEM. (C) T84, Caco-2 and LoVo cells were incubated in complete or nutrient-limited medium for 48h and collected for western blot for the protein levels of precursor and mature cathepsin B. Where indicated, the cells were also treated with 50nM bafilomycin A1 for 48h. (D) T84 cells were treated with complete or nutrient-limited medium for 24h and processed for -IF staining for cathepsin D and LAMP1. The scale bars correspond to 10  $\mu$ m. (E) Intensity profiles along a transect line traced over the image for both nutrient-rich and limited cells are shown. (F) Colocalization analysis was conducted using the Coloc2 plugin of Fiji with default settings, 5 images and 50 cells from each group were used. The mean Pearson's coefficient is given for each group. Statistical analysis was carried out using an unpaired *t*-test, except in (B) where ANOVA was used. \* $p < 0.05$ , \*\* $p < 0.01$ ; Baf A1, bafilomycin A1; Mature CatB, mature cathepsin B; NL, nutrient-limited; NR, nutrient-rich; ns, nonsignificant; Pro-CatB, precursor cathepsin B.

change in nutrient-rich or -limited cells, suggesting that under both conditions, the lysosomes were active (Figure 2F).

### 2.3 | Lysosomal Morphology and Biogenesis in Nutrient-Limited Cells

The lysosomal function is dependent on both the structure of lysosomes and their molecular characteristics. Therefore, the

morphology of lysosomes in nutrient-limited T84 cells was evaluated using immuno-electron microscopy imaging of T84 cells grown in the nutrient-limited medium for 24 h following the Tokuyasu method [24]. LAMP1 and LAMP2 markers were used to label the lysosomal membrane and cell morphology was evaluated with transmission electron microscopy (TEM). Giant lysosomes of around 1  $\mu\text{m}$  were observed near the nucleus in nutrient-limited T84 cells. Lysosomal size is known to be in the range of 0.2–0.3  $\mu\text{m}$  [25], suggesting that nutrient

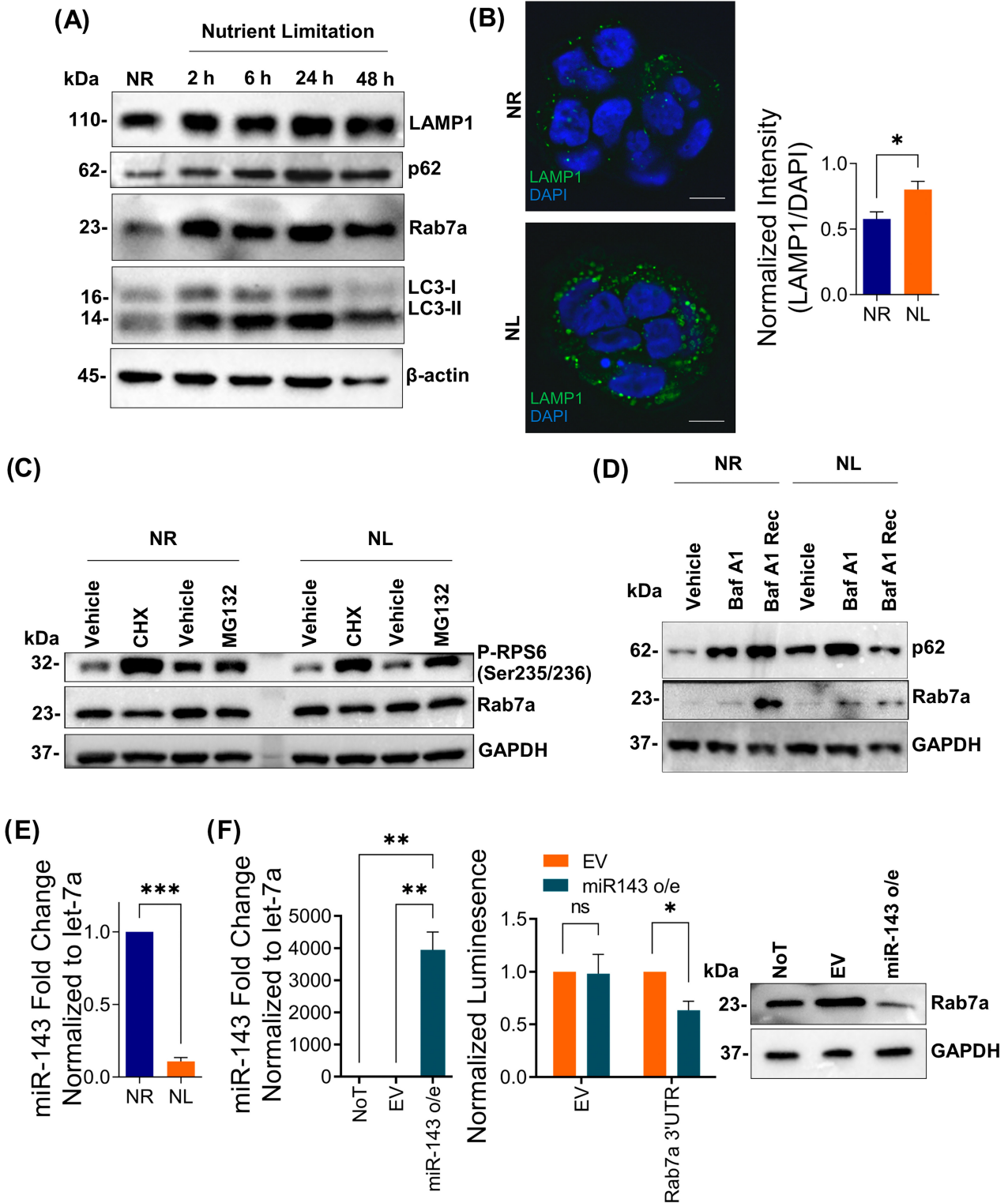


FIGURE 4 | Figure legend on next page.

limitation not only led to the perinuclear localization of the lysosomes but also resulted in a dramatic increase in their size (Figure 3A) [25].

Nutrient limitation can lead to the activation of lysosome biogenesis, by inside-out lysosomal signaling and activation of transcription factors such as TF-E3. Following its nuclear translocation, TF-E3 binds to the Coordinated Lysosomal Expression and Regulation (CLEAR) elements of the promoter regions of lysosomal and autophagic genes [26]. Immunofluorescence (IF) staining using a TF-E3 antibody showed significantly increased nuclear translocation in response to nutrient limitation in T84 cells (Figure 3B,C). These data are also in line with our observations on the elevated levels of autophagy proteins with nutrient limitation (Figure 1B). To further evaluate whether TF-E3 was transcriptionally active, mRNA levels of the CLEAR genes, *SQSTM1*, *BECN1*, *GABARAP*, *UVRAG*, *LAMP1*, *MCOLN1*, *RAB7A* and *CTSB*, were determined by qRT-PCR [27–29]. We observed a statistically significant increase in the expression of *SQSTM1*, *UVRAG*, *GABARAP*, *UVRAG*, *CTSB* and *LAMP1*, which supports the increased nuclear translocation of TF-E3. The expression of *MCOLN1* and *RAB7A* showed no significant difference between nutrient-rich and -limited cells (Figure 3D). Thus, the expression of all four autophagy genes evaluated was significantly increased, while the expression of two out of four lysosomal genes was enhanced in response to nutrient limitation. This suggests that nutrient limitation led to a stronger transcriptional upregulation of autophagy genes compared to lysosomal genes.

## 2.4 | Post-Transcriptional Regulation of the Endolysosomal Marker Rab7a in Nutrient-Limited Cells

To evaluate any temporal changes in lysosomal abundance with nutrient limitation, the levels of endolysosomal as well as autophagy markers were determined over a time course.

Starting from a time point as early as 2 h of limited nutrient availability, the protein levels of both autophagy and endolysosomal markers were remarkably increased (Figure 4A). The increase in lysosomal abundance after 48 h of nutrient limitation was also observed with IF staining using a LAMP1 antibody (Figure 4B). This high protein expression of LAMP1 was most likely to be transcriptionally regulated since both mRNA and protein levels of LAMP1 were increased with nutrient limitation (Figures 3D and 4A). Of note, the Rab7a protein level was seen to increase robustly as early as within 2 h of nutrient limitation while its mRNA levels remained unchanged (Figures 3D and 4A), pointing toward a rapid post-transcriptional regulation.

Release of stored Rab7a protein from stress granules was considered as a potential mechanism for the rapid increase in Rab7a protein levels in T84 cells upon nutrient limitation. However, we did not observe any formation of stress granules in nutrient-limited T84 cells whereas T84 cells treated with sodium arsenite (positive control) clearly showed the formation of stress granules (Figure S1F). Next, to evaluate whether the expression of Rab7a was regulated translationally or via delayed protein degradation, the nutrient-rich and -limited cells were treated with either cycloheximide (translation elongation inhibitor), MG132 (proteasome inhibitor) or bafilomycin A1 (lysosomal degradation inhibitor). Here, determination of Ribosomal Protein S6 (RPS6) phosphorylation served as a positive control since accumulation of intracellular amino acids following inhibition of protein synthesis activates mTORC1 as a feedback mechanism [30, 31]. Treatment of T84 cells with cycloheximide could modestly decrease the protein levels of Rab7a in both nutrient-rich and -limited cells (Figure 4C). Additionally, Rab7a protein turnover in nutrient-rich cells was most likely regulated in the lysosome rather than the proteasome since treatment of T84 cells with bafilomycin A1 led to a significant increase in Rab7a protein levels (Figure 4D) while MG132 treatment had no effect in either nutrient-rich or nutrient-limited cells (Figure 4C). Since cycloheximide treatment did not lead to a complete loss of

**FIGURE 4** | Effect of nutrient limitation on lysosomal abundance and expression of endolysosomal markers. (A) Time course showing an increase in the expression of endolysosomal and autophagy markers with 2–48 h of nutrient limitation. Images are representative of three independent biological replicates.  $\beta$ -Actin was used as an internal control, and fold changes were determined based on the expression in nutrient-rich cells. (B) IF image showing lysosomal abundance (LAMP1 staining) in T84 cells incubated in complete or nutrient-limited medium for 24 h. Scale bar corresponds to 10  $\mu$ m. The fluorescence intensity was normalized to DAPI. The bar graph represents the mean values of 5 different images and 50 cells. (C) T84 cells grown in nutrient-rich or nutrient-limited medium for 48 h were cotreated with either MG132 (10  $\mu$ M) or cycloheximide (20  $\mu$ g/mL) and processed for western blot. p-RPS6 (S235/236) served as a positive control for the treatments. GAPDH was used as a loading control. (D) T84 cells grown in nutrient-rich or nutrient-limited medium for 48 h were cotreated with bafilomycin A1 (100 nM) and collected for western blot. The image is representative of three independent replicates. GAPDH was used as a loading control. p62 served as a positive control for bafilomycin A1 treatment. The same p62 and GAPDH blots are also shown in Figure S1E. (E) Determination of mature miR-143 levels with 48 h nutrient limitation in T84 cells. *let-7a* was used as the internal control. Two independent replicates were carried out, and fold changes were determined by normalization to nutrient-rich cells. (F) Confirmation of targeting of Rab7a by miR-143 in HEK293 cells. The leftmost panel shows the confirmation of the miR-143 overexpression in HEK293 cells by miRNA-specific qRT-PCR. HEK293 cells were transiently transfected with pcDNA3.1/Neo\_miR143 vector or the corresponding empty vector (EV) for 24 h and processed for qRT-PCR. *let-7a* was used as internal control, two independent replicates were carried out, and fold changes were determined by normalization to untransfected HEK293 cells. The middle panel shows the targeting of the 3' UTR of RAB7A by miR-143. HEK293 cells overexpressing miR-143 or control were transfected with the pGWIZ RPS30M SuperNanoLuc Vector cloned with the 3' UTR of RAB7A or the corresponding EV. All cells were transfected with the pGWIZ RPS30M Firefly Vector for normalization. Right panel shows a western blot image confirming a decrease in Rab7a protein levels in HEK293 cells overexpressing miR-143. The image is representative of three biological replicates, GAPDH was used as a loading control. All densitometry analyses are shown in Figure S5. Statistical analysis was carried out using an unpaired *t*-test except Figure 4F where ANOVA was used. \* $p < 0.05$ , \*\* $p < 0.01$ , \*\*\* $p < 0.001$ ; EV, empty vector; miR-143 o/e, miR-143 overexpression; NL, nutrient-limited; NoT, no transfection, NR, nutrient-rich; ns, nonsignificant.



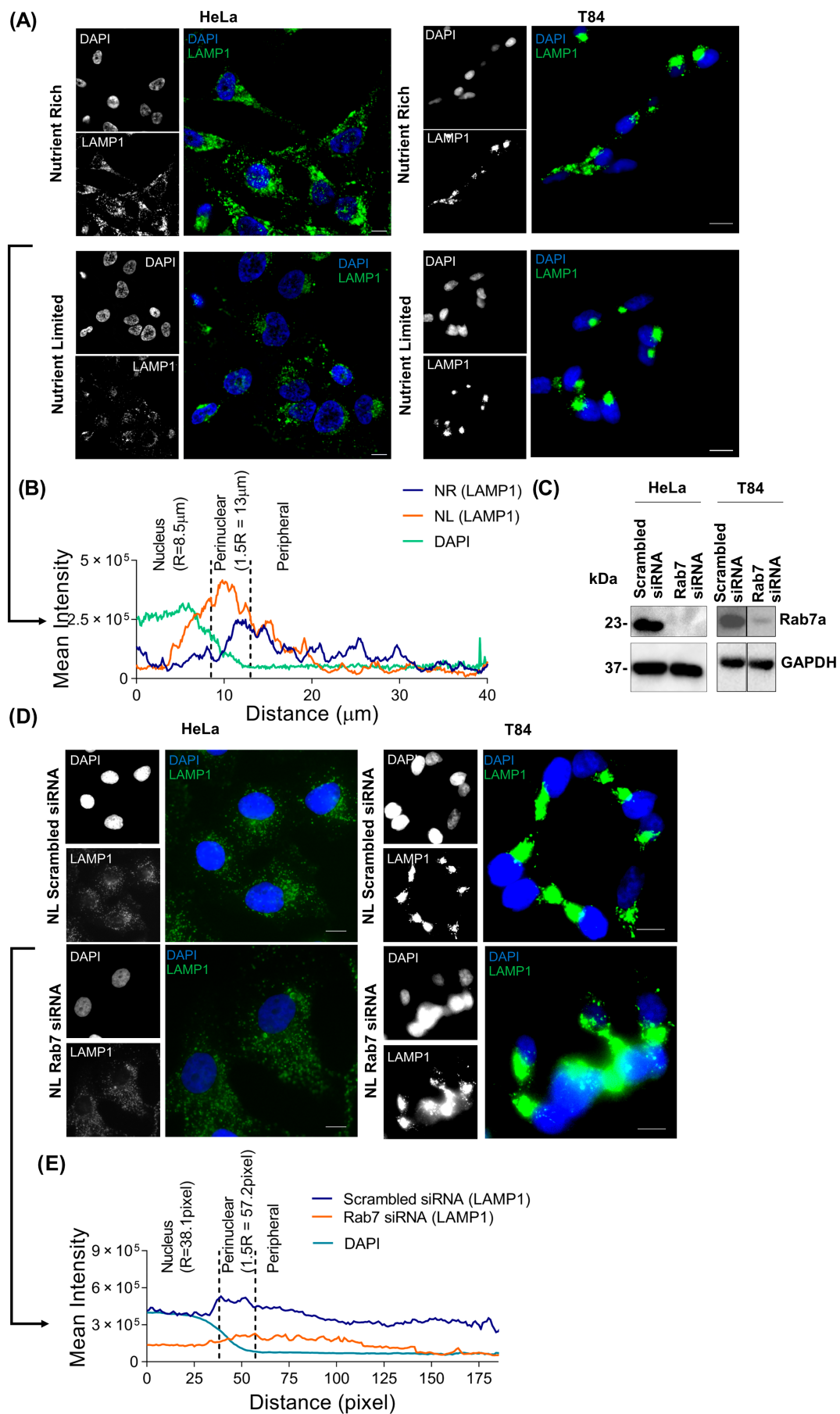


**FIGURE 5** | Figure legend on next page.



protein levels of Rab7a, we hypothesized the presence of additional regulation via the binding of regulatory molecules such as microRNAs.

A small RNA sequencing of nutrient-limited and rich cells indicated a significant loss of miR-143 in nutrient-limited compared to nutrient-rich cells, which could be confirmed by RT-qPCR (Figure 4E). miR-143-3p was predicted to target the RAB7A mRNA via multiple algorithms. To confirm this targeting, HEK293 cells were transfected with a luciferase reporter vector containing the 3' UTR of RAB7A along with a pcDNA3.1-miR143/Neo(miR-143) vector to overexpress miR-143-3p. Cells transfected with the empty luciferase vector showed no change in luminescence signal with miR-143 overexpression, whereas cells transfected with the vector containing the entire RAB7A 3' UTR sequence showed a statistically significant decrease in the luminescence signal (Figure 4F). To evaluate whether overexpression of miR-143 led to a decrease in the expression of RAB7A and HEK293 cells were transfected with the miR143 overexpression plasmid and were collected for western blot. A decrease in Rab7a protein level was observed with the overexpression of miR-143 (Figure 4F).

## 2.5 | Rab7a Orchestrates the Subcellular Localization of Lysosomes in Nutrient-Limited Cells

Several studies have reported that lysosomes can accumulate in the perinuclear region upon starvation [32–35]. Therefore, we first determined the subcellular localization of lysosomes in nutrient-limited T84 cells and observed a clear perinuclear localization (Figure 5A, right panel). A similar perinuclear localization is also very apparent in the nutrient-limited T84 cells stained with siRLysosome (Figure 2A). The large nucleus to total cell area ratio and their nature of growth in clusters precluded numerical evaluation of the distance of the lysosomes from the nucleus in T84 cells (Figure 5A). Preliminary experiments suggested that incubation of HeLa cells in the nutrient-limited medium also led to a perinuclear accumulation of lysosomes. These cells have a large cytoplasmic area which allowed the calculation of the distance of the lysosomes from the nucleus. In line with T84 cells, HeLa cells also exhibited high cell viability

in response to nutrient limitation (Figure S2A). The average radius of the nucleus in 40 HeLa cells was determined as 8.5  $\mu\text{m}$  (THUNDER Live-cell Imaging System) or 38.1 pixels (Nikon Eclipse 55i Fluorescent microscope) and the average perinuclear region was determined as up to 13  $\mu\text{m}$  (THUNDER Live-cell Imaging System) or 57.2 pixels (Nikon Eclipse 55i Fluorescent microscope) from the center of the nucleus. We observed that the lysosomes were distributed throughout the cytoplasm in nutrient-rich cells, while they were mainly localized at the perinuclear region in nutrient-limited cells (Figure 5A,B, left panel).

Rab7a can bind to adaptor proteins such as FYCO1 for association with the motor protein kinesin, whereas binding to the adaptor protein RILP enables Rab7a to be associated with the dynein complex. For the perinuclear movement of lysosomes, the dynein complex is functional, while the kinesin complex can be implicated in the wider peripheral distribution of lysosomes in the cytoplasm [36]. These associations suggest that Rab7a can mediate the subcellular localization of lysosomes. We therefore transiently silenced Rab7a in both T84 and HeLa cells using siRNA (Figure 5C). Indeed, we observed that lysosomes were collected at the perinuclear region in nutrient-limited HeLa and T84 cells transfected with scrambled siRNA, whereas the siRNA-mediated knockdown of Rab7a resulted in the distribution of lysosomes throughout the cytosol in both cell lines (Figure 5D). Quantitative analysis of the distance of the lysosomes from the nucleus could be carried out for HeLa cells only (Figure 5E) due to the large nucleus to total cell area ratio in T84 cells.

## 2.6 | Perinuclear Lysosomes in Nutrient-Limited Cells Trap Chemotherapy Drugs Contributing to Drug Resistance

We next evaluated the physiological significance of the perinuclear localization of lysosomes in the nutrient-limited cells and hypothesized a role in reduced sensitivity to drugs, possibly via their trapping in acidic perinuclear lysosomes. Using publicly available data from the Cancer Cell Line Encyclopedia (CCLE) data, we have analyzed 22 genes categorized under “Docking and fusion” by Bordi et al. [29] for resistance or

**FIGURE 5** | Evaluation of subcellular localization and morphology of lysosomes in response to nutrient limitation. (A) T84 and HeLa cells were treated with a complete or nutrient-limited medium for 24 h and processed for immunofluorescence staining with the LAMP1 antibody to determine the subcellular localization of lysosomes. The scale bar corresponds to 10  $\mu\text{m}$ . (B) Quantitative representation of the localization of lysosomes in response to nutrient limitation. Forty different HeLa cells were used to determine the radius of the nucleus and perinuclear region. Purple and orange colored lines show the mean intensity of the signal collected in the green channel in nutrient-rich and -limited HeLa cells respectively, while the green colored line shows the mean intensity of the signal collected in the DAPI channel over a line drawn from the center of the nucleus to the edges of the cells. (C) Confirmation of the knockdown of Rab7a. HeLa and T84 cells were transfected with 10 nM of scrambled or Rab7a-specific siRNA in Opti-MEM medium for 24 h, followed by 24 h of nutrient limitation. Total protein was isolated from the siRNA-transfected cells and a western blot was carried out for Rab7a. GAPDH served as a loading control. Image is representative for two biological replicates. The image for T84 cells was taken from two separate lanes in the same membrane that were spliced together. These bands are also shown in Figure 7B. (D) Silencing of Rab7a resulted in a redistribution of lysosomes in nutrient-limited HeLa and T84 cells. Both cell lines were transfected with Rab7a siRNA or scrambled siRNA and processed for immunofluorescence staining with the LAMP1 antibody. The scale bar corresponds to 10  $\mu\text{m}$ . (E) Quantitative evaluation of lysosomal localization in Rab7a silenced nutrient-limited HeLa cells. Forty different cells were used to determine the radius of the nucleus and perinuclear region. Purple and orange colored lines show the mean intensity of the signal collected in the green channel in scrambled and Rab7a siRNA-transfected HeLa cells, respectively, while the green colored line shows the mean intensity of the signal collected in the DAPI channel over a line drawn from the center of the nucleus to the edges of the cells. Two different microscopes were used for the imaging analysis: THUNDER Live-cell Imaging System (A, B,  $\mu\text{m}$  scale) and Nikon Eclipse 55i Fluorescent microscope (D, E, pixel scale). NL, nutrient-limited; NR, nutrient-rich.

sensitivity to 550 compounds [37]. We observed that Rab7a was in a cluster of genes showing the most resistance to the drugs (Figure 6A). These data suggest that among the endosomal/lysosomal trafficking proteins, Rab7a was one of the

genes with the strongest association with drug resistance. Lipophilic or weakly basic drugs are known to be sequestered in the lysosomes via nontransporter-mediated mechanisms [10]. Doxorubicin was shown to form a cluster around the

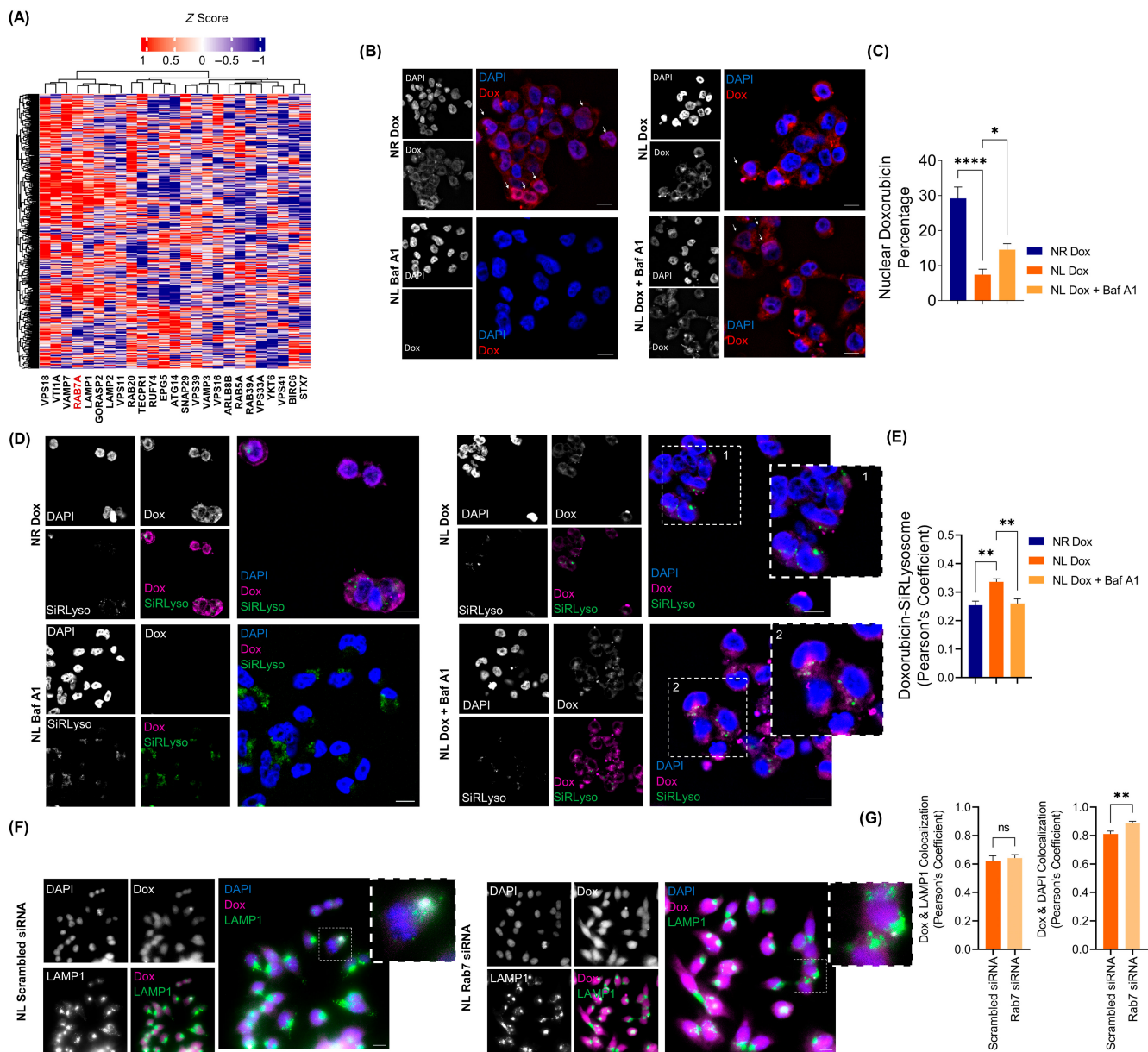


**FIGURE 6** | Evaluation of the accumulation of doxorubicin within lysosomes with nutrient limitation. (A) Heatmap showing Pearson correlation coefficients between 550 compounds and the expression 22 genes related to “docking and fusion” of lysosomes [29] in 47 CRC cell lines. Positive Z scores correspond to higher drug resistance. Rab7a was located in a cluster of proteins with the highest resistance to the 550 compounds (B) Decreased accumulation of doxorubicin in the nucleus of nutrient-limited T84 cells, which could be reversed with lysosomal alkalization. T84 cells were treated with 10  $\mu$ g/mL of doxorubicin and/or 100 nM bafilomycin A1 for 24 h in nutrient-rich or nutrient-limited medium and processed for immunofluorescence staining. The scale bar corresponds to 10  $\mu$ m. (C) Bar graph represents the mean nuclear doxorubicin intensities of at least 5 different images and 200 cells. (D) Lysosomal trapping of doxorubicin. T84 cells were treated with nutrient-limited medium containing 10  $\mu$ g/mL of doxorubicin and/or 100 nM bafilomycin A1 for 24 h and processed for immunofluorescence staining with siRlysosome. The scale bar corresponds to 10  $\mu$ m. (E) Colocalization analysis was conducted using Coloc2 plugin of Fiji with default settings, 100 cells from each of the three groups of cells were analyzed. The mean Pearson's coefficient was calculated to determine lysosomal trapping. (F) Loss of nuclear doxorubicin with the silencing of Rab7a. T84 cells were incubated with a Rab7a or scrambled siRNA for 24 h in a complete medium followed by fixation and staining for doxorubicin or LAMP1. (G) A significant increase in the nuclear signal of doxorubicin was observed in Rab7a silenced T84 cells compared to the scrambled siRNA-transfected cells. No significant change in the colocalization of LAMP1 and doxorubicin was observed between Rab7a silenced and control cells. Statistical analysis was carried out using ANOVA for (C, E) and unpaired *t*-test for (G). \**p* < 0.05, \*\**p* < 0.01, \*\*\*\**p* < 0.0001. Baf A1, bafilomycin A1; Dox, doxorubicin; NL, nutrient-limited; NR, nutrient-rich.

perinuclear region in doxorubicin-resistant MCF-7 cells, indicating that the drug was sequestered in acidic lysosomes, while the sensitive cells showed accumulation of the drug inside the nucleus where it is functional [13]. However, it is currently unknown whether perinuclear lysosomes in nutrient-limited cells can also trap drugs. To determine this, we firstly determined the colocalization of doxorubicin with the nuclear marker DAPI in T84, Caco-2 and LoVo cells. The fluorescent signal of doxorubicin colocalized with the DAPI signal in about 30% of the nutrient-rich cells (Figure 6B,C) confirming the nuclear accumulation of the drug. With nutrient limitation, we observed the strongest decrease in nuclear accumulation of doxorubicin in T84 cells, followed by Caco-2 cells; LoVo cells retained most of the doxorubicin in the nucleus with nutrient limitation (Figures 6B,C and S2E). The loss of nuclear accumulation of doxorubicin could be partially reversed when the nutrient-limited T84 cells were treated with bafilomycin A1 (Figure 6B,C). Additionally, doxorubicin showed a significantly higher colocalization with siRLysosome in the nutrient-limited T84 cells, suggesting that the drug could be trapped inside active lysosomes (Figure 6D,E). Sequestration of doxorubicin in active lysosomes was significantly decreased when the lysosomes were alkalinized with bafilomycin A1 (Figure 6D,E). We also evaluated the colocalization of doxorubicin with the lysosomal marker LAMP1 when Rab7a was silenced in nutrient-rich T84 cells. We did not observe any significant difference in the colocalization of LAMP1 with doxorubicin between control and Rab7a-silenced cells; however, we did observe a significant increase in the colocalization of doxorubicin with the nuclear dye DAPI in cells where Rab7a was silenced (Figure 6F,G).

Lysosomal alkalinization did not lead to nuclear doxorubicin levels to a level comparable to nutrient-rich cells (Figure 6C). Therefore, we hypothesized the presence of additional mechanisms such as the activation of efflux pumps in nutrient-limited cells. In fact, we observed a remarkable increase in the expression of the drug efflux pump MDR1, but not MRP1 in the nutrient-limited cells (Figure S2B). This suggests that nutrient limitation in T84 cells can activate multiple mechanisms for drug resistance that include, but may not be limited to lysosomal trapping and drug efflux.

## 2.7 | Re-Sensitization of Nutrient-Limited Cells to Chemotherapy Drugs With Alkalinization of the Lysosome

We next determined whether the trapping of drugs in the lysosome can affect the sensitivity of nutrient-limited cells to drugs such as 5-FU. For this, the proliferation of T84, Caco-2 and LoVo cells treated with 5-FU and doxorubicin alone or in combination with bafilomycin A1 was determined with an MTT assay (Figure S2C). Nutrient-limited T84 cells showed significantly less viability when treated with a combination of bafilomycin A1 and 5-FU compared to 5-FU alone (Figure S2C). The loss in viability in nutrient-limited cells was accompanied by a decrease in the expression of the replication marker PCNA with the combination of low dose 5-FU (10  $\mu$ M) and bafilomycin A1 (100 nM) compared to treatment with the individual agents in nutrient-limited T84 cells (Figure 7A) as well as nutrient-limited

cells with Rab7a silenced (Figure 7B). A similar decrease in cell viability was observed in HeLa cells incubated in the nutrient-limited medium. Although HeLa cells were highly sensitive to doxorubicin, a further decrease in cell viability was observed when the cells were treated with doxorubicin in combination with bafilomycin A1 (Figure S2D). The Loewe additivity model indicated that the decrease in cell viability in nutrient-limited T84 cells treated with bafilomycin A1 and 5-FU was synergistic, with a mean synergy score of 10.54 (Figure 7C) [38]. The scores in LoVo (2.57) and Caco-2 (3.12) cells did not reach the threshold of > 10 to be considered as a synergistic effect. Additionally, a colony formation assay confirmed that nutrient-limited T84 cells had lower sensitivity to 5-FU; lysosomal alkalinization with bafilomycin A1 in the nutrient-limited cells could increase their sensitivity to 5-FU to a greater extent compared to the nutrient-rich cells (Figures 7D and S2F).

We next evaluated whether lysosomal alkalinization could sensitize nutrient-limited cells to 5-FU in vivo. For this, microtumors were generated on the chorioallantoic membrane (CAM) using nutrient-rich or -limited T84 cells treated with 5-FU alone, bafilomycin A1 alone, or a combination of both drugs on the chicken CAM. The microtumor volume of nutrient-limited cells treated with 5-FU was larger than the microtumor volume of nutrient-rich cells treated with 5-FU indicating a better tolerance (more resistance) of the chemotherapy agent with nutrient limitation (Figure 7E). Ki67 positivity in the tumors was comparable in nutrient-rich and -limited cells treated with vehicle or 5-FU (Figure S3A,B). When bafilomycin A1 was used in combination with 5-FU in the nutrient-limited cells, higher sensitivity to 5-FU treatment was observed, as indicated by a near-significant decrease in tumor volume ( $p=0.0642$ ) (Figure 7E) and a significant decrease in Ki67 staining ( $p=0.0129$ ) (Figure S3A,B). Of note, a high number of blood vessels was observed around the microtumor in both nutrient-rich and nutrient-limited cells treated with 5-FU alone. The vascularization of the tumors appeared to decrease remarkably when cells were treated with bafilomycin A1 (Figure S3C). This is supported by a previous observation of blood vessel normalization in a multiple melanoma model in which the lysosomotropic agent chloroquine could alter the trafficking of Notch1 and its signaling in endothelial cells, thereby leading to normalization of vessels in an autophagy-independent manner [39]. To confirm that the decrease in tumor size was related to the alkalinization of lysosomes and not the inhibition of autophagy, we treated nutrient-rich and limited T84 cells with the autophagy inhibitor 3-methyladenine (3MA). First, the proliferation of T84 cells in the presence of 5-FU alone and in combination with 3MA was evaluated with an MTT assay and was found to be highly comparable (Figure S3D) and quite contrary to the combinatorial effect observed with bafilomycin A1 (Figure S2C). This indicates that rather than inhibition of autophagy, modulation of lysosomal acidity was more important to regulate susceptibility to chemotherapy agents.

## 3 | Discussion

Cancer cells at the core of solid tumors have less access to nutrients mostly due to poor vasculature [40]. To survive the harsh microenvironment, these cells rewire their metabolism and







signaling pathways to enhance survival via the upregulation of nutrient transporters, enhanced nutrient biosynthesis and an increase in nutrient recycling [41].

In this study, we have aimed to mechanistically investigate how cancer cells respond to the limited availability of major nutrient sources (glucose, glutamine and serum). Cells that have a low supply of nutrients (such as at the core of the tumor) are likely to either die or activate stress signaling that can enable survival [42]. We observed that nutrient-limited T84, Caco-2 and LoVo cells showed the activation of AMPK and autophagy pathways as well as the inhibition of mTORC1, as expected, along with high viability both in vitro and in vivo, suggesting that these cell lines may activate stress mitigation pathways for survival.

Nutrient-limited T84, LoVo and Caco-2 cells showed an increase in the accumulation of the autophagy cargo protein p62. Although the accumulation of p62 is generally associated with impaired flux, we observed that the protein levels of p62 were increased further when all three cell lines were treated with bafilomycin A1, suggesting the presence of a functional autophagic flux. The observed increase in protein levels of p62 can be attributed to the increase in the mRNA expression of *SQSTM1* (encoding p62) in the nutrient-limited cells. Lysosomal acidity and activity confer the cells with various advantages to cope with nutrient stress [8]. We, therefore, evaluated lysosomal activity with siRLysosome, cathepsin B cleavage, LysoTracker and cathepsin D lysosomal localization and observed a significant and reproducible increase in acidity and/or abundance of lysosomes upon nutrient limitation in T84 cells with all of the techniques. Moreover, evaluation of the subcellular structure by EM revealed a remarkable change in the morphology of the lysosomes with the appearance of giant lysosomes located near the nucleus. Although the accumulation of enlarged lysosomes is mostly associated with impaired acidity or activity such as in lysosomal storage disorders, our data suggests that nutrient-limited T84 cells had large, catalytically active lysosomes that were most likely not consumed during autophagy. During autophagy, the degraded lysosomes are generally restored by autophagic lysosome reformation (ALR); [43, 44] however, mTOR was inactive for the duration of nutrient limitation (48 h) in T84 cells suggesting that ALR was not activated in these cells.

Lysosomal biogenesis involves the synthesis of structural and functional elements of lysosomes to form an integrated organelle [45, 46]. Lysosome reformation is critical to ensure lysosomal homeostasis in cells following the degradation of autophagic cargo since the degradation process drains the pool of lysosomes in the cells [26]. For the de novo formation of lysosomes, TF-E3 is a major transcription factor that can bind to the CLEAR elements at the promoters of target genes [27, 45]. Under nutrient-rich conditions, active mTORC1 phosphorylates TF-E3 and prevents its nuclear translocation via interaction with the cytosolic chaperone 14-3-3 proteins [47]. Under low nutrient availability, mTORC1 is inhibited, and/or the Ca<sup>2+</sup>-calmodulin-dependent protein phosphatase calcineurin is activated leading to the dephosphorylation of TF-E3, preventing its interaction with the 14-3-3 chaperone and enabling its nuclear translocation. Nutrient-limited T84 cells showed nuclear translocation of TF-E3, supporting the inhibition of mTOR signaling and increased lysosomal acidity, elevated LAMP1 protein levels, and increased lysosome size. Six out of eight CLEAR genes analyzed (*SQSTM1*, *BECN1*, *GABARAP*, *UVRAG*, *LAMP1* and *CTSB*) showed an increase in mRNA expression supporting the nuclear translocation and transcriptional activity of TF-E3 while the mRNA expression of *MCOLN1* and *RAB7A* showed no change.

The CLEAR gene Rab7a is an endolysosomal trafficking G protein that is involved in the fusion of late endosomes and lysosomes, as well as autophagosomes and lysosomes [48, 49]. Nutrient-limited cells are known to have highly acidic lysosomes that are generally more perinuclear [22, 33, 34]. Rab7a can regulate the positioning of lysosomes in cells [36, 50, 51]. We, therefore, evaluated the protein expression of Rab7a in nutrient-rich and -limited T84 cells and observed a robust increase with nutrient limitation, starting from as early as 2h of nutrient limitation, pointing toward rapid post-transcriptional regulation. Small RNA sequencing analysis of nutrient-limited cells suggested a decrease in miR-143 levels upon nutrient limitation. We confirmed that Rab7a could be targeted with miR-143; thus, the remarkable increase in the protein levels of Rab7a with no change in the mRNA expression in nutrient-limited cells could have resulted, at least in part, from the downregulation of miR-143. Opposed to a more dispersed localization in the cytoplasm in nutrient-rich cells, we observed a perinuclear localization

**FIGURE 7** | Effects of nutrient limitation on the response of CRC cells to chemotherapy agents. (A) A decrease in the protein levels of PCNA was observed in response to a combinatorial treatment of T84 cells with bafilomycin A1 and 5-FU compared to either agent alone. GAPDH served as the internal control; the image is representative of two independent biological replicates. (B) A decrease in the protein levels of PCNA was observed in nutrient-limited T84 cells silenced for Rab7a and treated with 5-FU compared to scrambled siRNA-transfected cells treated with 5-FU. The bands obtained with Rab7a and GAPDH antibody using proteins from Rab7a silenced and scrambled siRNA-transfected cells (Lanes 3 and 5) are also shown in Figure 5C. Densitometry analyses are shown in Figure S5. (C) The Loewe additivity model, generated with SynergyFinder 3, shows a synergistic effect of 5-Fluorouracil and bafilomycin A1. A score > 10 is indicative of synergy, which was observed only in the T84 cells. (D) Colony formation assay showing increased sensitivity of nutrient-limited T84 cells to a combination of 5-FU and bafilomycin A1. T84 cells treated with 50 μM 5-FU alone or in combination with 100 nM bafilomycin A1 either in nutrient-rich or -limited medium for 48 h. The bar graph represents the average of three biological replicates ± SEM. (E) Near-significant decrease ( $p=0.064$ ) in microtumor volume generated with nutrient-limited T84 cells treated with both 5-Fluorouracil and bafilomycin A1 compared to either agent alone. T84 cells were incubated with a nutrient-rich or nutrient-limited medium for 48 h. Where indicated, the cells were cotreated with 50 μM 5-FU and/or 100 nM bafilomycin A1 for the duration of incubation. The microtumors were excised and the volume was determined. Statistical analysis was carried out using ANOVA. \* $p < 0.05$ , \*\* $p < 0.01$ , \*\*\* $p < 0.001$ , \*\*\*\* $p < 0.0001$ . 5-FU, 5-fluorouracil; Baf A1, bafilomycin A1; NL, nutrient-limited; NR, nutrient-rich.

of lysosomes upon nutrient limitation, which we hypothesized could be orchestrated by Rab7a. In fact, silencing of Rab7a led to dramatic relocalization of the lysosomes from the perinuclear region to a more uniform distribution throughout the cytoplasm in both T84 and HeLa cells, suggesting that the increased protein levels of Rab7a can lead to rapid relocalization of the lysosomes upon nutrient limitation.

Enlarged, abundant lysosomes that are perinuclearly located were shown to be involved in a process known as lysosomal trapping/sequestration [11]. In this, lipophilic, weakly basic drugs are trapped in lysosomes via nontransporter-mediated mechanisms [10]. We hypothesized that the giant acidic lysosomes in nutrient-limited cells could contribute toward trapping of chemotherapy drugs and thereby enhance drug resistance. 5-FU inhibits the nucleotide synthetic enzyme thymidylate synthase and limits the availability of deoxythymidine triphosphate (dTTP), which can inhibit DNA replication and repair [52]. We observed that all nutrient-limited colon cancer cells showed high viability with 5-FU compared to the cells grown in the nutrient-rich medium. The combination of bafilomycin A1, an agent that alkalinizes the lysosomes, with a low dose of 5-FU resulted in decreased proliferation, as evidenced by a decrease in the expression of the DNA replication protein PCNA in nutrient-limited T84 cells in vitro along with a significantly smaller microtumor volume and low Ki67 staining in vivo. Silencing of Rab7a, which resulted in a relocalization of the lysosomes toward the cell periphery also remarkably led to a decrease in PCNA levels. These data suggest that acidic perinuclearly located lysosomes were necessary for the resistance of these cells to 5-FU when grown under nutrient-limited conditions. We next carried out a Loewe additivity model and observed that the effect of bafilomycin A1 was synergistic with 5-FU in T84 cells, with a mean synergy score of 10.54.

To further substantiate these data, we determined the subcellular localization of the fluorescent chemotherapy agent doxorubicin in nutrient-rich and -limited T84 cells. We observed that the fluorescent signal of doxorubicin was mainly colocalized with DAPI (nuclear dye) in nutrient-rich cells. This is expected since doxorubicin is a DNA intercalating agent that inhibits the function of Topoisomerase II and thereby causes cell death [53]. The nuclear localization of doxorubicin showed a modest but significant decrease in nutrient-limited cells, which could be partially reversed with the use of bafilomycin A1. Of note, we observed lysosomal accumulation of doxorubicin in the nutrient-limited T84 cells, as evidenced by increased colocalization with siRLysosome (a marker for active lysosomes) which could also be reversed upon treatment with bafilomycin A1. Moreover, the silencing of Rab7a led to an increase in the nuclear localization of doxorubicin; however, we did not observe any change in the colocalization of LAMP1 and doxorubicin in the Rab7a silenced versus control cells. Overall, these data suggest that accumulation of chemotherapy drugs in acidic perinuclear lysosomes can occur in nutrient-limited T84 cells, yet not all the lysosomes in which doxorubicin was accumulated were active.

Although nutrient limitation resulted in a dramatic decrease in the nuclear localization of doxorubicin, alkalinization of

the lysosomes did not lead to a complete restoration of the drug to the nucleus. We therefore examined other potential mechanisms for resistance. Multidrug resistance (MDR) is the primary mechanism by which cancer cells acquire resistance to chemotherapy regimens [54]. MDR is mostly mediated by the overexpression of the ATP-binding cassette (ABC) transporter proteins which function in an ATP-dependent efflux of drugs [55]. The ABCB1 (*MDR1*) gene product P-gp and ABCC1 gene product MRP1 are the major ABC transporters known to be involved in MDR [56]. We evaluated the mRNA levels of *MDR1* and *MRP1* in nutrient-limited T84 cells and observed a robust increase in the expression of *MDR1*, but not *MRP1*. These data suggest that nutrient limitation could lead to the activation of multiple mechanisms for drug resistance in cancer cells.

Overall, we showed that the limitation of major nutrient sources such as glucose, glutamine and serum-activated signaling enhanced lysosomal numbers and activity; the lysosomes, in turn, could trap drugs causing the cells to acquire resistance to chemotherapy agents. This resistance could be reversed with the simple use of a lysosomal inhibitor along with chemotherapy agents such as 5-FU and doxorubicin.

## 4 | Materials and Methods

### 4.1 | Cell Culture and Nutrient Limitation

T84, Caco-2, LoVo, HEK293 and HeLa cells were cultured as described in [Supporting Information](#). For nutrient limitation, the cells were incubated for 48 h in glucose and glutamine-free DMEM (T84, Caco-2 and HeLa) or glucose and glutamine-free RPMI (LoVo and HEK293) supplemented with 1% FBS, 0.1 g/L glucose and 0.2 mM L-glutamine and 1% penicillin/streptomycin. The medium for T84, Caco-2 and HeLa was also supplemented with 1 mM sodium pyruvate and 0.1 mM nonessential amino acids. Caco-2 and T84 cells can undergo confluency-dependent differentiation and were therefore cultured at subconfluency. More details are provided in [Supporting Information](#).

### 4.2 | Drug/Chemical Treatments

The drugs and chemicals used in the current study are shown in [Supporting Information: Methods](#). For drug treatments of 24 h duration, the cells were first incubated in the nutrient-limited medium for 24 h followed by the treatment in the nutrient-limited medium for a further 24 h. The total duration of treatment or nutrient limitation did not exceed 48 h.

### 4.3 | Plasmids and Cloning

pGWIZ RPS30M SuperNanoLuc (RAB7A 3' UTR sequence cloned) luciferase reporter vector and pGWIZ RPS30M firefly vector (for normalization) were used in the Luciferase Reporter Assays to confirm the targeting of Rab7a by miR-143. The SuperNanoLuc EV and the firefly vector were obtained as a kind gift from Dr. Khalid S Khabar (King Faisal University, Saudi

Arabia). pcDNA3.1/Neo vector, which was a kind gift from Prof. Dr. Elif Erson Bensan (METU, Ankara), and was used to clone and overexpress miR-143. The details of the cloning protocol are provided in the [Supporting Information](#).

#### 4.4 | RNA Isolation, cDNA Synthesis and qRT-PCR

RNA was isolated from 70% to 80% confluent cells incubated in a nutrient-limited or nutrient-rich medium and/or treated with different drugs using the Macherey Nagel RNA isolation kit. For qRT-PCR, the RNA was treated with DNase I, converted to cDNA, and quantified by qPCR. Further details and primer sequences are provided in [Supporting Information](#).

#### 4.5 | Isolation of miRNA and miRNA qRT-PCR

Small RNAs were isolated from nutrient-limited or rich Caco-2 cells using the mirVana miRNA Isolation Kit (Thermo Fisher Scientific) in accordance with the manufacturer's instructions. Small RNA sequencing was carried out at the Beijing Genome Institute. To determine miRNA levels, a qRT-PCR protocol was applied as described previously [57]. The details of the protocol and the primer sequences are provided in the [Supporting Information](#).

#### 4.6 | siRNA-Mediated Silencing of RAB7A

A pool of four siRNAs targeting RAB7A (Dharmacon) along with its scrambled siRNA control was used. HeLa and T84 cells were transfected with siRNA using Lipofectamine RNAiMAX Transfection Reagent (Thermo Fischer Scientific). Please see the [Supporting Information](#) for more details.

#### 4.7 | Protein Isolation and Western Blot

Proteins were isolated from 70% to 80% confluent cells incubated in a nutrient-rich or nutrient-limited medium using an MPER protein isolation kit (Promega) and a combination of hypotonic buffer and RIPA Buffer supplemented with protease and phosphatase inhibitors for total and cytoplasmic/nuclear protein extraction, respectively. Western blotting was carried out with 15–20 µg of protein using standard techniques. Further details and a list of antibodies are provided in [Supporting Information](#).

#### 4.8 | Proliferation and Viability Assays

Cells ( $1 \times 10^4$  cells/well) were seeded in a complete medium and left for attachment overnight. The following day, the cells were washed with PBS and then incubated for 48 h in either a complete or nutrient-limited medium, and the cells were collected by trypsinization for the relevant assay. Count and Viability Assay (Muse), Trypan Blue Exclusion Assay, MTT and colony formation assays were applied as described in [Supporting Information](#). To determine any synergism between chemotherapeutic agents and bafilomycin A1 treatment SynergyFinder 3.0 web tool was employed using default settings [38].

#### 4.9 | LysoTracker and siRLysosome Staining

For the evaluation of the LysoTracker signal by imaging, T84, Caco-2 and LoVo cells ( $1.2 \times 10^5$ /well) were seeded in 6-well plates and incubated in the nutrient-rich or nutrient-limited medium for 48 h plus vehicle or 50 nM bafilomycin A1. Upon completion of treatment, the cells were stained with 50 nM of LysoTracker Red DND-99 (Thermo Fisher Scientific) for 30 min at 37°C in PBS and DAPI as described in [Supporting Information](#). The cells were imaged in a FLoid Imaging Station (Thermo Fisher Scientific).

For siRLysosome staining, T84, Caco-2 and LoVo cells were incubated in nutrient-rich or nutrient-limited medium in the presence or absence of bafilomycin A1 (50 nM) for 48 h. At the end of the incubation, the active lysosomes were stained with siRLysosome (1 µM, SpiroChrom) for 3 h and imaged in a THUNDER Live-cell Imaging System.

#### 4.10 | IF Imaging

T84, HEK293 or HeLa cells ( $6 \times 10^4$  cells/well) were seeded onto sterile, 12–15 mm glass coverslips placed into 12-well plates in complete medium and left for attachment overnight. The following day, the cells were washed with PBS, and treatments indicated in the figure legends were applied for 24 h. Upon completion of the treatment, cells were fixed in 4% paraformaldehyde and processed for incubation in a primary antibody, followed by incubation with an Alexa Fluor conjugated secondary antibody. Counterstaining was carried out with DAPI. Further details and the list of antibodies used are provided in [Supporting Information](#).

#### 4.11 | Immunogold EM Imaging

The immuno-EM experiments were performed following the Tokuyasu method as reported previously [58]. T84 cells were seeded in T25 flasks in complete medium and left for attachment overnight. The following day, the cells were washed with PBS and incubated in the nutrient-limited medium for 24 h. Further details and the list of antibodies used are provided in [Supporting Information](#).

#### 4.12 | Chorioallantoic Membrane Assay and Immunohistochemistry Staining

Fertilized specific-pathogen-free Leghorn eggs were obtained from Tavukçuluk Araştırma Enstitüsü (Ankara, Türkiye) or VALO Biomedica (Osterholz-Scharmbeck, Germany). On the ninth day of embryonic development,  $1 \times 10^6$  viable cell pellets (determined with a Trypan Blue exclusion assay) obtained after incubation in the nutrient-limited or nutrient-rich medium (+/- any indicated drugs) for 48 h were collected in 20 µL medium, mixed with 20 µL Matrigel (Corning) and placed on the CAM of the developing embryos. The eggs were placed in an incubator at 37°C at 60%–70% humidity and incubated for another 5 days, after which the microtumors were harvested for volume measurement or embedding for immunohistochemistry. For further details please see [Supporting Information](#).



The harvested tumors were processed for immunohistochemical staining for hematoxylin and eosin after deparaffinization. Details on antibody dilutions and histological assessment are provided in the [Supporting Information](#).

#### 4.13 | Drug Correlation Analyses

Raw read counts of colon cancer cell lines ( $n=47$ ) were downloaded from the CCLE portal (<https://portals.broadinstitute.org/ccle/data>) and normalized with the DESeq2 package [59]. VST-transformed read counts for 22 genes related to the “docking and fusion” of lysosomes [29] were extracted and used for correlation analysis with the drug sensitivity data. Drug sensitivity values (area under the curve [AUC]) for 550 compounds were downloaded from the National Cancer Institute database [37]. Pearson  $r$  coefficients were normalized and plotted using the ComplexHeatmap R library [60] with Euclidean distance and the “ward.D” linkage method. The details of the analyses can be found in [Supporting Information](#).

#### 4.14 | Statistical Analysis

Each experiment contains at least two biological replicates, each having at least two technical replicates. For data analysis, GraphPad Prism 6 (GraphPad Software Inc) was used. To evaluate significance, one-way ANOVA followed by the Sidak multiple comparisons test or an unpaired  $t$ -test was used. Statistical significance was defined as a  $p$  value of less than 0.05.

#### Acknowledgments

Experiments: A.E.G.T., H.H.H., Z.E.S., G.O., N.S.M., C.H., K.H. and I.S. with supervision from R.S.-S, N.L. and S.B. Study design: A.E.G.T., H.H.H. and S.B. Manuscript writing: A.E.G.T., R.S.-S, K.H., N.L. and S.B. Pathological data analysis: K.E.-W. and A.A. Funding acquisition and overall supervision: S.B. The study was funded by TÜBİTAK project 118Z116 and TEZ-D-108-2020-10258 (BAP, ODTÜ) to S.B. and A.E.G.T. was supported by an EMBO Scientific Exchange Grant 9424 to UMC Utrecht. A.E.G.T., H.H.H., G.O. and N.S.M. were supported by TUBITAK BİDEB 2210 and 2211. We sincerely thank Dr. Ayşe Elif Erson Bensan (Orta Doğu Teknik University, Türkiye), Dr. Onur Çizmecioglu (İhsan Doğramacı Bilkent University, Türkiye), Dr. Soner Doğan (Yeditepe University, Türkiye) and Dr. Menekşe Ermiş Şen (Terasaki Institute) for sharing resources and useful discussions.

#### Conflicts of Interest

The authors declare no conflicts of interest.

#### Data Availability Statement

The data underlying Figure 4E is available in Table S1. Public domain information: These data were derived from the following resources at the CCLE portal (<https://portals.broadinstitute.org/ccle/data>), National Cancer Institute database ([https://ctd2data.nci.nih.gov/Public/Broad/CTRPv2.0\\_2015\\_ctd2\\_ExpandedDataset/](https://ctd2data.nci.nih.gov/Public/Broad/CTRPv2.0_2015_ctd2_ExpandedDataset/)). Privacy/ethical restrictions: The data that support the findings of this study are available on request from the corresponding author. The data are not publicly available due to privacy or ethical restrictions. Included in the article: The data that support the findings of this study are available in the methods of this article.

#### Peer Review

The peer review history for this article is available at <https://www.webofscience.com/api/gateway/wos/peer-review/10.1111/tra.12956>.

#### References

1. S. Y. Lunt and M. G. Vander Heiden, “Aerobic Glycolysis: Meeting the Metabolic Requirements of Cell Proliferation,” *Annual Review of Cell and Developmental Biology* 27 (2011): 441–464.
2. N. Lee and D. Kim, “Cancer Metabolism: Fueling More Than Just Growth,” *Molecules and Cells* 39 (2016): 847–854.
3. M. G. V. Heiden, L. C. Cantley, and C. B. Thompson, “Understanding the Warburg Effect: The Metabolic Requirements of Cell Proliferation,” *Science* 209, no. 324 (1979): 1029–1033.
4. N. N. Pavlova and C. B. Thompson, “The Emerging Hallmarks of Cancer Metabolism,” *Cell Metabolism* 23 (2016): 27–47.
5. A. Muir and M. G. Vander Heiden, “The Nutrient Microenvironment Affects Cancer Therapy,” *Science* 360 (2018): 962–963.
6. L. Yu, Y. Chen, and S. A. Tooze, “Autophagy Pathway: Cellular and Molecular Mechanisms,” *Autophagy* 14 (2018): 207–215.
7. H. Xu and D. Ren, “Lysosomal Physiology,” *Annual Review of Physiology* 77 (2015): 57–80.
8. T. Tang, Z. Y. Yang, D. Wang, et al., “The Role of Lysosomes in Cancer Development and Progression,” *Cell & Bioscience* 10 (2020): 1–18.
9. C. Fennelly and R. K. Amaravadi, “Lysosomal Biology in Cancer,” *Methods in Molecular Biology* 1594 (2017): 293–308.
10. B. Zhitomirsky and Y. G. Assaraf, “Lysosomal Sequestration of Hydrophobic Weak Base Chemotherapeutics Triggers Lysosomal Biogenesis and Lysosomedependent Cancer Multidrug Resistance,” *Oncotarget* 6 (2015): 1143–1156.
11. J. Hraběta, M. Belhajová, H. Šubrtová, M. A. M. Rodrigo, Z. Heger, and T. Eckschlagner, “Drug Sequestration in Lysosomes as One of the Mechanisms of Chemoresistance of Cancer Cells and the Possibilities of Its Inhibition,” *International Journal of Molecular Sciences* 21 (2020): 4392.
12. S. Llanos, D. Megias, C. Blanco-Aparicio, et al., “Lysosomal Trapping of Palbociclib and Its Functional Implications,” *Oncogene* 38 (2019): 3886–3902.
13. B. Guo, A. Tam, S. A. Santi, and A. M. Parissenti, “Role of Autophagy and Lysosomal Drug Sequestration in Acquired Resistance to Doxorubicin in MCF-7 Cells,” *BMC Cancer* 16 (2016): 1–18.
14. L. L. Qing, X. W. Jun, D. Pan, H. Chen, and L. Zhang, “Inhibition of Autophagy by Bafilomycin A1 Promotes Chemosensitivity of Gastric Cancer Cells,” *Tumor Biology* 37 (2016): 653–659.
15. T. Kawaguchi, K. Miyazawa, S. Moriya, et al., “Combined Treatment With Bortezomib Plus Bafilomycin A1 Enhances the Cytocidal Effect and Induces Endoplasmic Reticulum Stress in U266 Myeloma Cells: Crosstalk Among Proteasome, Autophagy-Lysosome and ER Stress,” *International Journal of Oncology* 38 (2011): 643–654.
16. P. Maycotte, S. Aryal, C. Ct, and J. Thorburn, “Chloroquine Sensitizes Breast Cancer Cells to Chemotherapy Independent of Autophagy,” *Autophagy* 8 (2012): 200–212.
17. E. B. Golden, H. Y. Cho, A. Jahanian, et al., “Chloroquine Enhances Temozolomide Cytotoxicity in Malignant Gliomas by Blocking Autophagy,” *Neurosurgical Focus* 37 (2014): 1–11.
18. H. H. Hüsnügil, A. E. Gulec Taskiran, İ. Guderer, et al., “Lysosomal Alkalinization in Nutrient Restricted Cancer Cells Activates Cytoskeletal Rearrangement to Enhance Partial Epithelial to Mesenchymal Transition,” *Translational Oncology* 41 (2024): 101860.



19. G. A. Pastorino, I. Sheraj, K. Huebner, et al., "A Partial Epithelial-Mesenchymal Transition Signature for Highly Aggressive Colorectal Cancer Cells That Survive Under Nutrient Restriction," *Journal of Pathology* 262 (2024): 347–361.
20. P. D. Pezze, S. Ruf, A. G. Sonntag, et al., "A Systems Study Reveals Concurrent Activation of AMPK and mTOR by Amino Acids," *Nature Communications* 7 (2016): 1–19.
21. C. Mauvezin and T. P. Neufeld, "Bafilomycin A1 Disrupts Autophagic Flux by Inhibiting Both V-ATPase-Dependent Acidification and Ca-P60A/SERCA-Dependent Autophagosome-Lysosome Fusion," *Autophagy* 11 (2015): 1437–1438.
22. D. J. Klionsky, D. J. Klionsky, K. Abdelmohsen, et al., "Guidelines for the Use and Interpretation of Assays for Monitoring Autophagy (3rd Edition)," *Autophagy* 12 (2016): 1–222.
23. W. Kenneth, M. M. K. Dunn, and J. H. McDonald, "A Practical Guide to Evaluating Colocalization in Biological Microscopy," *American Journal of Physiology. Cell Physiology* 300 (2011): 723–742.
24. J. W. Slot and H. J. Geuze, "Cryosectioning and Immunolabeling," *Nature Protocols* 2, no. 10 (2007): 2480–2491.
25. P. C. Trivedi, J. J. Bartlett, and T. Pulini, "Lysosomal Biology and Function: Modern View of Cellular Debris Bin," *Cells* 9 (2020): 1–35.
26. C. Yang and X. Wang, "Lysosome Biogenesis: Regulation and Functions," *Journal of Cell Biology* 220 (2021): 1–15.
27. M. Palmieri, S. Impey, H. Kang, et al., "Characterization of the CLEAR Network Reveals an Integrated Control of Cellular Clearance Pathways," *Human Molecular Genetics* 20 (2011): 3852–3866.
28. B. Pan, H. Zhang, T. Cui, and X. Wang, "TFEB Activation Protects Against Cardiac Proteotoxicity via Increasing Autophagic Flux," *Journal of Molecular and Cellular Cardiology* 113 (2017): 51–62.
29. M. Bordin, R. De Cegli, B. Testa, R. A. Nixon, A. Ballabio, and F. Cecconi, "A Gene Toolbox for Monitoring Autophagy Transcription," *Cell Death & Disease* 12 (2021): 1044.
30. T. Watanabe-Asano, A. Kuma, and N. Mizushima, "Cycloheximide Inhibits Starvation-Induced Autophagy Through mTORC1 Activation," *Biochemical and Biophysical Research Communications* 445 (2014): 334–339.
31. A. Beugnet, A. R. Tee, P. M. Taylor, and C. G. Proud, "Regulation of Targets of mTOR (Mammalian Target of Rapamycin) Signalling by Intracellular Amino Acid Availability," *Biochemical Journal* 372 (2003): 555–566.
32. X. Li, N. Ryzewski, A. Hider, et al., "A Molecular Mechanism to Regulate Lysosome Motility for Lysosome Positioning and Tubulation," *Nature Cell Biology* 18 (2016): 404–417.
33. C. Erie, M. Sacino, L. Houle, M. L. Lu, and J. Wei, "Altered Lysosomal Positioning Affects Lysosomal Functions in a Cellular Model of Huntington's Disease," *European Journal of Neuroscience* 42 (2015): 1941–1951.
34. G. P. Starling, Y. Y. Yip, A. Sanger, P. E. Morton, E. R. Eden, and M. P. Dodding, "Folliculin Directs the Formation of a Rab34–RILP Complex to Control the Nutrient-Dependent Dynamic Distribution of Lysosomes," *EMBO Reports* 17 (2016): 823–841.
35. V. I. Korolchuk, S. Saiki, M. Lichtenberg, et al., "Lysosomal Positioning Coordinates Cellular Nutrient Responses," *Nature Cell Biology* 13 (2011): 453–460.
36. D. E. Johnson, P. Ostrowski, V. Jaumouillé, and S. Grinstein, "The Position of Lysosomes Within the Cell Determines Their Luminal pH," *Journal of Cell Biology* 212 (2016): 677–692.
37. M. G. Rees, B. Seashore-Ludlow, J. H. Cheah, et al., "Correlating Chemical Sensitivity and Basal Gene Expression Reveals Mechanism of Action," *Nature Chemical Biology* 12 (2016): 109–116.
38. A. Ianevski, A. K. Giri, and T. Aittokallio, "SynergyFinder 3.0: An Interactive Analysis and Consensus Interpretation of Multi-Drug Synergies Across Multiple Samples," *Nucleic Acids Research* 50 (2022): W739–W743.
39. H. Maes, A. Kuchnio, A. Peric, et al., "Tumor Vessel Normalization by Chloroquine Independent of Autophagy," *Cancer Cell* 26 (2014): 190–206.
40. W. Palm, "Metabolic Plasticity Allows Cancer Cells to Thrive Under Nutrient Starvation," *Proceedings of the National Academy of Sciences of the United States of America* 118 (2021): 1–3.
41. M. R. Sullivan and M. G. Vander Heiden, "Determinants of Nutrient Limitation in Cancer," *Critical Reviews in Biochemistry and Molecular Biology* 54 (2019): 193–207.
42. R. J. Gillies, J. S. Brown, A. R. A. Anderson, and R. A. Gatenby, "Eco-Evolutionary Causes and Consequences of Temporal Changes in Intratumoural Blood Flow," *Nature Reviews. Cancer* 18 (2018): 576–585.
43. A. P. Lieberman, R. Puertollano, N. Raben, S. Slaugenhaupt, S. U. Walkley, and A. Ballabio, "Autophagy in Lysosomal Storage Disorders," *Autophagy* 8 (2012): 719–730.
44. Y. Chen and L. Yu, "Recent Progress in Autophagic Lysosome Reformation," *Traffic* 18 (2017): 358–361.
45. L. E. Karageorgos, E. L. Isaacs, D. A. Brooks, et al., "Lysosomal Biogenesis in Lysosomal Storage Disorders," *Experimental Cell Research* 234 (1997): 85–97.
46. J. Klumperman and G. Raposo, "The Complex Ultrastructure of the Endolysosomal System," *Cold Spring Harbor Perspectives in Biology* 6 (2014): 1–22.
47. T. T. Dang and S. H. Back, "Translation Inhibitors Activate Autophagy Master Regulators TFEB and TFE3," *International Journal of Molecular Sciences* 22 (2021): 12083.
48. C. Bucci, P. Thomsen, P. Nicoziani, J. McCarthy, and B. Van Deurs, "Rab7: A Key to Lysosome Biogenesis," *Molecular Biology of the Cell* 11 (2000): 467–480.
49. S. Meresse, J. P. Gorvel, and P. Chavrier, "The Rab7 GTPase Resides on a Vesicular Compartment Connected to Lysosomes," *Journal of Cell Science* 108 (1995): 3349–3358.
50. F. Guerra and C. Bucci, "Multiple Roles of the Small GTPase Rab7," *Cells* 5 (2016): 1–28.
51. J. Pu, C. M. Guardia, T. Keren-Kaplan, and J. S. Bonifacio, "Mechanisms and Functions of Lysosome Positioning," *Journal of Cell Science* 129 (2016): 4329–4339.
52. D. B. Longley, D. P. Harkin, and P. G. Johnston, "5-Fluorouracil: Mechanisms of Action and Clinical Strategies," *Nature Reviews. Cancer* 3 (2003): 330–338.
53. A. G. Patel and S. Kaufmann, "How Does Doxorubicin Work?," *eLife* 1 (2012): 1–3.
54. E. T. Bin, A. Shahriar, A. R. Mahmud, et al., "Multidrug Resistance in Cancer: Understanding Molecular Mechanisms, Immunoprevention and Therapeutic Approaches," *Front Oncologia* 12 (2022): 1–38.
55. E. M. Leslie, R. G. Deeley, and S. P. C. Cole, "Multidrug Resistance Proteins: Role of P-Glycoprotein, MRP1, MRP2, and BCRP (ABCG2) in Tissue Defense," *Toxicology and Applied Pharmacology* 204 (2005): 216–237.
56. K. Sodani, A. Patel, R. J. Kathawala, and Z. S. Chen, "Multidrug Resistance Associated Proteins in Multidrug Resistance," *Chinese Journal of Cancer* 31 (2012): 58–72.
57. S. Cirera and P. K. Busk, "Quantification of miRNAs by a Simple and Specific qPCR Method," *Methods in Molecular Biology (Clifton, N.J.)* 1182 (2014): 73–81.

58. J. Fermie, L. de Jager, H. E. Foster, et al., “Bimodal Endocytic Probe for Three-Dimensional Correlative Light and Electron Microscopy,” *Cell Reports Methods* 2 (2022): 1–17.
59. M. I. Love, W. Huber, and S. Anders, “Moderated Estimation of Fold Change and Dispersion for RNA-Seq Data With DESeq2,” *Genome Biology* 15 (2014): 550.
60. Z. Gu, R. Eils, and M. Schlesner, “Complex Heatmaps Reveal Patterns and Correlations in Multidimensional Genomic Data,” *Bioinformatics* 32 (2016): 2847–2849.

### Supporting Information

Additional supporting information can be found online in the Supporting Information section.